SCIENTIFIC REPORT

Casaletti Massimiliano, NEWFOCUS grant n. 3482

Purpose of the visit

The major objective of the work was to develop an efficient full wave analysis code for the analysis of Substrate Integrated Waveguides (SIW) structures. They are realized using standard printed circuit board (PCB) technology which is easy and cheap to produce. The basic idea is to realize waveguide channels on a grounded dielectric slab by using arrays of metallic vias. SIW technology maintains the advantage of metallic waveguides in addition with the possibility of integration typical of microstrip structures, allowing sophisticated packaging technology and the integration of complex beam-forming networks and antennas on the same boards. The analysis of the propagation in SIW configurations has been carried out in many ways; however because of the presence of vias fence which form the lateral walls of the waveguide, a finite difference of finite element type of solution needs to be often employed. Thus the design of real device using quasi-optical system (electrically very large structure) can be time consuming and memory demanding.

Description of the work carried out during the visit

The analysis of large structures using conventional waveguide has been performed in an efficient way by using the method of the moments, thanks to the availability of the waveguide Green's function: SIW structures are modelled as an ensemble of cylindrical scatterers used to design waveguides, reflectors, feeder, etc., inside Parallel Plate Waveguides (PPW) coupled through slots. Using the equivalence principle it was possible to decompose the whole structure as a set of Parallel Plate Waveguide (PPW) structure feed by equivalent magnetic sources.
The field inside the waveguide structure has been decomposed as the superposition of an incident field (the field radiated by the source in the homogeneous PPW) and the field scattered by the dielectric or metallic posts:

$$\mathbf{H} = \mathbf{H}_{inc} + \mathbf{H}_{s} \tag{1}$$

Each of these simplified sub-problems has been studied by a method of the moment technique making use of an efficient Green's function for the PPW.
Since all the vias have cylindrical shape the natural way to proceed was to express the incident field as a cylindrical wave vectors expansion. This allows us to impose easily the boundary condition on every cylinder since every component of the incident field was conformal to the scatterer surfaces.

The work has been divided in four successive steps:
1. Efficient analysis of the field radiated by a source in a PPW.
2. Efficient evaluation of the scattered field by metallic vias inside the PPW.

1. Efficient analysis of the field radiated by a source in a PPW

In the first step, the field inside each waveguide structure has been efficiently computed by considering the dyadic Green's function of the PPW expressed as an expansion in terms of vectorial cylindrical eigenfunctions.

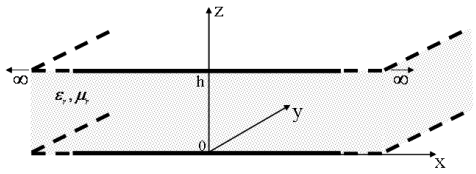

Figure 1. Parallel plate waveguide geometry.

The magnetic field radiated by a magnetic source $\mathbf{M}_s$ defined over S' is thus given by

$$\mathbf{H}_{inc}(\mathbf{r}) = -j\omega\varepsilon \int_{S'} \underline{\underline{\mathbf{G}}}^{(1)}(\mathbf{r},\mathbf{r}')\mathbf{M}_s(\mathbf{r}')d\mathbf{r}' \tag{2}$$

where $\underline{\underline{\mathbf{G}}}^{(1)}$ is the primary dyadic Green's function, $\mathbf{r}$ is the observation point and $\mathbf{r}'$ is the source position.

We have considered two perfect conductive plates are placed at $z=0$ and $z=d$ and filled by a uniform dielectric medium described by ε,μ (see fig.1). Following the procedure introduced in [10][11] the primary dyadic Green's function $\underline{\underline{\mathbf{G}}}^{(1)}$ can be obtained from two scalar functions ℓ' and ℓ'' representing respectively the TM a TE components with respect to the z axis direction as

$$\begin{aligned} -j\omega\mu\underline{\underline{\mathbf{G}}}^{(1)}(\mathbf{r},\mathbf{r}') &= k^2(\nabla\times\hat{\mathbf{z}})(\nabla'\times\hat{\mathbf{z}})\ell'(\mathbf{r},\mathbf{r}') \\ &+(\nabla\times\nabla\times\hat{\mathbf{z}})(\nabla'\times\nabla'\times\hat{\mathbf{z}})\ell''(\mathbf{r},\mathbf{r}')-\left(\hat{\mathbf{z}}\hat{\mathbf{z}}+\frac{\nabla_t\nabla_t}{\nabla_t^2}\right)\delta(\mathbf{r}-\mathbf{r}') \end{aligned} \tag{3}$$

where $k=\sqrt{\varepsilon\mu}$, ∇ and ∇' denote a gradient operator with respect to observation location and source location, respectively and $\nabla_t = \nabla - \frac{\partial}{\partial z}\hat{\mathbf{z}}$ denotes the transverse gradient operator.

The scalar functions introduced above are related to the scalar Green's function G by the relations

$$\begin{aligned} -\nabla_t^2\ell'(\mathbf{r},\mathbf{r}') &= G'(\mathbf{r},\mathbf{r}') \\ -\nabla_t^2\ell''(\mathbf{r},\mathbf{r}') &= G''(\mathbf{r},\mathbf{r}') \end{aligned} \tag{4}$$

where both G', G'' are solution of the scalar wave equation

$$(\nabla^2+k^2)G(\mathbf{r},\mathbf{r}') = -\delta(\mathbf{r},\mathbf{r}') \tag{5}$$

but are subjected to TM or TE boundary condition on the PEC plate surface, respectively:

$$\left.\frac{\partial}{\partial z}G'(\mathbf{r},\mathbf{r}')\right|_{z=0,h}=0$$
$$\left.G''(\mathbf{r},\mathbf{r}')\right|_{w=0,h}=0 \tag{6}$$

Solving (5) in cylindrical coordinates using a radial waveguide representation, imposing conditions (6), and then inserting the expression of ℓ' and ℓ'' in (3) we obtain the final expression

$$\underline{\underline{\mathbf{G}}}^{(1)}(\mathbf{r},\mathbf{r}')=-\left(\hat{\mathbf{z}}\hat{\mathbf{z}}+\frac{\nabla_t\nabla_t}{\nabla_t^2}\right)\delta(\mathbf{r}-\mathbf{r}')-\sum_{m=0}^{+\infty}\sum_{n=-\infty}^{\infty}(-1)^n\left(1-\frac{\delta_{m0}}{2}\right)$$
$$\cdot\frac{k}{2\omega\varepsilon k_{\rho_m}^2 h}\left[\begin{matrix}\mathbf{M}_n\left(k_{\rho_m},k_{z_m},\boldsymbol{\rho},z\right)\mathbf{M}_n'\left(k_{\rho_m},k_{z_m},\boldsymbol{\rho}',z'\right)\\+\mathbf{N}_n\left(k_{\rho_m},k_{z_m},\boldsymbol{\rho},z\right)\mathbf{N}_n'\left(k_{\rho_m},k_{z_m},\boldsymbol{\rho}',z'\right)\end{matrix}\right] \tag{7}$$

Where $k_{z_m}=\frac{m\pi}{h}$, and δ_{m0} is the Kronecker's delta function, $\mathbf{M}_n$, $\mathbf{N}_n$ are cylindrical vectors eigenfunctions defined as [12]

$$\mathbf{M}_n=\begin{cases}\nabla\times\hat{\mathbf{z}}H_n^{(2)}\left(k_{\rho_m}\rho\right)e^{-jn\phi}\cos\left(k_{z_m}z\right) & \rho>\rho'\\ \nabla\times\hat{\mathbf{z}}J_n\left(k_{\rho_m}\rho\right)e^{-jn\phi}\cos\left(k_{z_m}z\right) & \rho\le\rho'\end{cases}$$
$$\mathbf{N}_n=\begin{cases}\frac{1}{k}\nabla\times\nabla\times\hat{\mathbf{z}}H_n^{(2)}\left(k_{\rho_m}\rho\right)e^{-jn\phi}\sin\left(k_{z_m}z\right) & \rho>\rho'\\ \frac{1}{k}\nabla\times\nabla\times\hat{\mathbf{z}}J_n\left(k_{\rho_m}\rho\right)e^{-jn\phi}\sin\left(k_{z_m}z\right) & \rho\le\rho'\end{cases} \tag{8}$$

and $\mathbf{M}_n'$, $\mathbf{N}_n'$ can be obtained from (8) by inverting $\rho>\rho'$ with $\rho\le\rho'$.

The first kind dyadic Green's function have been thus expressed as a cylindrical wave vectors expansion, but it presents an extra term when compared to other formulations presented in [12]. When $\mathbf{r}=\mathbf{r}'$ the delta-Dirac term cancels the spurious singularity coming from the differentiation of the scalar functions. Such an aspect is very important for the self-admittance evaluation.

The second kind dyadic Green's function has been obtained from (7) as

$$\underline{\underline{\mathbf{G}}}^{(2)}(\mathbf{r},\mathbf{r}')=\frac{1}{j\omega\varepsilon}\nabla\times\underline{\underline{\mathbf{G}}}^{(1)}(\mathbf{r},\mathbf{r}') \tag{9}$$

with the help of the wave-vectors properties $\nabla\times\mathbf{M}_n=k\mathbf{N}_n$, $\nabla\times\mathbf{N}_n=k\mathbf{M}_n$ [12].

2. Efficient evaluation of the scattered field by metallic vias inside the PPW

The second step of the problem was to determine the scattered field by the metallic pins

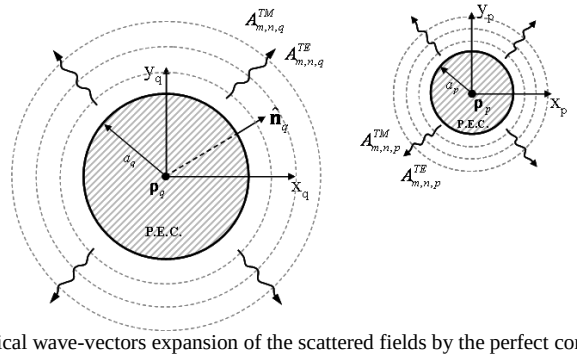

Figure 2. Cylindrical wave-vectors expansion of the scattered fields by the perfect conducting cylinders.

We have conssider N_p metallic vias centered at $\boldsymbol{\rho}_1, \boldsymbol{\rho}_2, \ldots, \boldsymbol{\rho}_{N_p}$ and a magnetic surface current density $\mathbf{M}_s$. The scattered field from each via has been expressed as a linear superposition of cylindrical wave as

$$\mathbf{H}_s(\mathbf{r}) = \sum_{p=1}^{N_p} \sum_{m=1}^{+\infty} \sum_{n=-\infty}^{+\infty} A^{TM}_{m,n,p} \mathbf{M}_n\left(k_{\rho_m}, k_{z_m}, \boldsymbol{\rho} - \boldsymbol{\rho}_p, z\right) + A^{TE}_{m,n,p} \mathbf{N}_n\left(k_{\rho_m}, k_{z_m}, \boldsymbol{\rho} - \boldsymbol{\rho}_p, z\right) \tag{10}$$

where the wave vectors outgoing expression has been used ($\mathbf{M}_n$, $\mathbf{N}_n$ defined with the second kind Hankel function) and the *m* and *n* indexes span over the vertical and horizontal dependences, respectively.
To determinate the scattered fields amplitude $A^{TM}_{m,n,p}$, $A^{TE}_{m,n,p}$ we have impose the boundary condition that the tangential electric field to be zero at the surface of the q-th via, namely

$$\hat{\mathbf{n}}_q \times \nabla \times \left(\mathbf{H}_{inc} + \mathbf{H}_s\right)\Big|_{|\boldsymbol{\rho} - \boldsymbol{\rho}_q| = a_q} = 0 \tag{11}$$

where $\hat{\mathbf{n}}_q$ is the normal unit vector to the surface and a_q is the radius of the via (see fig. 2).
Since the scatterer is conformal to the coordinate system, (11) can be solved separately for the TM and TE polarization.
Any cylindrical wave has been centered in the q-th pin local reference system by the help of the Bessel summation theorem.

$$H^{(2)}_n\left(k_{\rho_m}\left|\boldsymbol{\rho} - \boldsymbol{\rho}_p\right|\right) e^{-jn\phi_p} = \sum_{r=-\infty}^{+\infty} (-1)^{n-r} H^{(2)}_{n-r}\left(k_{\rho_m}\left|\boldsymbol{\rho}_q - \boldsymbol{\rho}_p\right|\right) \cdot J_r\left(k_{\rho_m}\left|\boldsymbol{\rho} - \boldsymbol{\rho}_q\right|\right) e^{-jr\phi_q} e^{-j(n-r)\varphi_{qp}} \tag{12}$$

where ϕ_p, ϕ_q and φ_{qp} angles are depicted in Fig. 3.

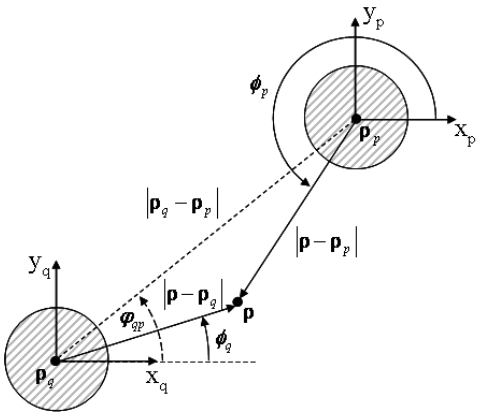

Figure 3. Via's local coordinate systems.

.

Using relations (7) ,(10) and (12) in (11), we obtained for the TM case:

$$\sum_{p=1,p\neq q}^{N_p}\sum_{n=-\infty}^{+\infty} A_{m,n,p}^{TM} T_{q,r,m,p,n}^{TM} + A_{m,r,p_q}^{TM} = E_{q,r,m}^{TM} \qquad T_{q,r,m,p,n}^{TM} = \frac{J_r\left(k_{\rho_m} a_q\right)}{H_r^{(2)}\left(k_{\rho_m} a_q\right)} H_{n-r}^{(2)}\left(k_{\rho_m}\left|\boldsymbol{\rho}_q - \boldsymbol{\rho}_p\right|\right) e^{-j(n-r)\varphi_{pq}}$$

$$E_{q,r,m}^{TM} = \omega\varepsilon \frac{J_r\left(k_{\rho_m} a_q\right)}{H_r^{(2)}\left(k_{\rho_m} a_q\right)} \frac{(-1)^r\left(1-\frac{\delta_{m0}}{2}\right)}{2k_{\rho_m}^2 h} \int_{S'} \boldsymbol{M}'_{-r}\left(k_{\rho_m}, k_{z_m}, \boldsymbol{\rho}' - \boldsymbol{\rho}_q, z'\right) \cdot \boldsymbol{M}_s\left(\boldsymbol{r}'\right) dr' \tag{5}$$

While for the TE case, we obtained

$$\sum_{p=1,p\neq q}^{N_p}\sum_{n=-\infty}^{+\infty} A_{m,n,p}^{TE} T_{q,r,m,p,n}^{TE} + A_{m,r,p_q}^{TE} = E_{q,r,m}^{TE} \qquad T_{q,r,m,p,n}^{TE} = \frac{J_r'\left(k_{\rho_m} a_q\right)}{H_r^{(2)\prime}\left(k_{\rho_m} a_q\right)} H_{n-r}^{(2)}\left(k_{\rho_m}\left|\boldsymbol{\rho}_q - \boldsymbol{\rho}_p\right|\right) e^{-j(n-r)\varphi_{pq}}$$

$$E_{q,r,m}^{TE} = \omega\varepsilon \frac{J_r'\left(k_{\rho_m} a_q\right)}{H_r^{(2)\prime}\left(k_{\rho_m} a_q\right)} \frac{(-1)^r\left(1-\frac{\delta_{m0}}{2}\right)}{2k_{\rho_m}^2 h} \int_{S'} \boldsymbol{N}'_{-r}\left(k_{\rho_m}, k_{z_m}, \boldsymbol{\rho}' - \boldsymbol{\rho}_q, z'\right) \cdot \boldsymbol{M}_s\left(\boldsymbol{r}'\right) dr' \tag{6}$$

The operation has been repeated for all the cylinders. As a consequence, 2m matrix equations have been solved.

Description of the main results obtained

The theory developed during the project has been implemented in a Matlab code.
As a first test the transmission characteristic of a coaxially fed waveguide [13] has been considered. The comparison of the same quantity computed with HFSS is reported in Fig.4. A good agreement with HFSS can been obtained using 5 cylindrical wave-vectors.

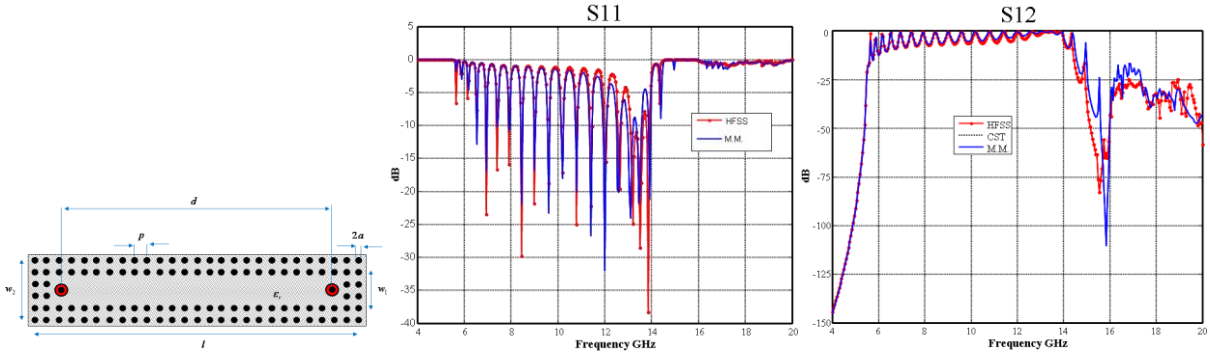

(a) (b) (c)

Figure 4. (a) Waveguide coaxially fed geometry: $\varepsilon_r = 4.3$ h=3.2mm $d = 100mm$ $p = 0.851mm$ $l = 119.6mm$ $p = 4.6mm$ $w_1 = 13.8mm$ $w_2 = 23mm$ $a = 0.83mm$; (b) Amplitude of the S11 parameter; (b) Amplitude of the S12 parameter.

As a second case a dual coupled cavity filter based on circular resonator [14] has been considered (Fig. 5.a). The simulation has been carried out using 5 cylindrical modes. The results obtained by our method and those obtained by HFSS are shown in Fig. 5.b, and they are in a good agreement.

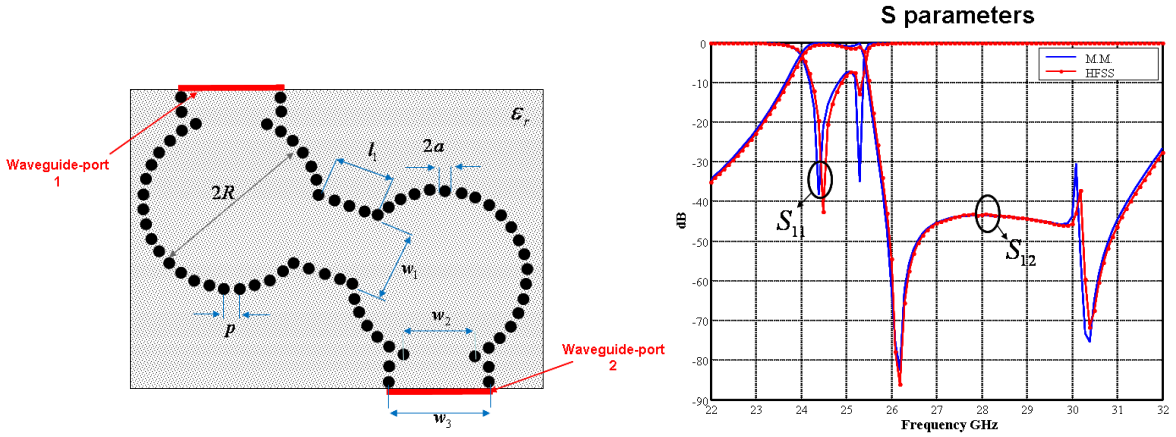

(a) (b)

Figure 5. (a) Dual cavity filter geometry $\varepsilon_r = 2.2$ h=0.5mm $w_1 = 4.08mm$ $w_2 = 9.93mm$ $w_3 = 5.50mm$ $a = 0.2mm$ $p = 0.851mm$ $l_1 = 3.404mm$ $R = 4.83mm$ $a = 2.55mm$; (b) Amplitude of the S parameters

In table I, CPU time for the considered cases are reported and compared to those needed to HFSS. As can be seen the algorithm is quite efficient.

Structure	N. cylinders	HFSS		This method
		Meshing time	Freq. point	Freq. point
Coaxially fed waveguide	*118*	*475 s*	*151 s*	*3 s*
Dual cavity filter	*116*	*130 s*	*14 s*	*4.5 s*

Project publications

M. Casaletti, R. Sauleau, M. Ettorre , S. Maci, “Mode Matching Method for the Analysis of Substrate Integrated Waveguides”, invited paper at the international conference 6th European Conference on Antennas and Propagation (EuCAP 2012) that will be held in Prague on 26-30 March 2012.

References

[1] L. Felsen, *Radiation and scattering of waves,* IEEE Press.
[2] W. C. Chew, *Waves and Field in Inhomogeneous Media*. New York: IEEE Press, 1995.
[3] J. J. Simpson, A. Taflove, J. A. Mix, and H. Heck, “Computational and experimental study of a microwave electromagnetic bandgap structure with waveguiding defect for potential use as bandpass wireless interconnect,” *IEEE Microw. Wireless Compon. Lett*., vol. 14, no. 7, pp. 343–345, Jul. 2004.
[4] H. J. Tang and W. Hong, “Substrate integrated waveguide dual mode filter with circular cavity,” in *Joint Int. Infrared Millimeter Waves/Terahertz Electron*. Conf., Shanghai, China, Sep. 2006, pp. 399–399.